Alma Mater Studiorum · Università di Bologna

Scuola di Scienze
Dipartimento di Fisica e Astronomia
Corso di Laurea in Fisica

Combined use of Drift Tubes and Resistive Plate Chamber information in the CMS Muon Barrel Trigger

Relatore:
Dott. Luigi Guiducci

Correlatore:
Dott. Carlo Battilana

Presentata da:
Marco Lorusso

Anno Accademico 2017/2018

Abstract

Il TwinMux è un sistema di elettronica digitale parte del trigger per muoni della regione centrale del rivelatore Compact Muon Solenoid al Large Hadron Collider del CERN di Ginevra. L'algoritmo del TwinMux produce segmenti di traccia combinando le informazioni ricostruite a livello delle singole stazioni di rivelatori Drift Tubes e Resistive Plate Chambers.

In questo lavoro sono state studiate le principali caratteristiche dell'algoritmo analizzando un campione di dati acquisito dal rivelatore durante il run protone-protone del 2018, e si è proceduto ad un confronto tra i segmenti prodotti in hardware e quelli prodotti dall'emulatore software dell'algoritmo. Si è osservato un buon accordo per le principali categorie di tracce prodotte dal sistema, dell'ordine del 99% in media, valore appropriato considerando l'utilizzo dell'emulatore nelle simulazioni Montecarlo. Infine, sono state individuate le principali tipologie di discrepanza che potrebbero essere risolte per migliare ulteriormente la simulazione.

Contents

Introduction

The Compact Muon Solenoid (CMS) is a general purpose experiment operating at the Large Hadron Collider (LHC) at CERN. In its outer part, CMS is equipped with a muon spectrometer built using three different types of gaseous detector technologies, arranged redundantly in multiple layers to maximize detection efficiency. Drift Tubes Chambers (DT) and Cathode Strip Chambers (CSC) cover, respectively, the barrel and the end-cap regions of the muon system and serve both as offline tracking and triggering devices. Resistive Plate Chambers (RPC) complement both DT and CSC and are mostly used in the trigger. The CMS muon spectrometer ensures efficient muon identification and improves the transverse momentum (p_T) measure of high energy muons. In addition, it provides a robust trigger system, able to identify the origin of a muon candidate in terms of LHC bunch crossing and perform a standalone measurement of its p_T.

The CMS trigger is staged into two levels, called Level-1 Trigger (L1T) and High-Level Trigger (HLT). The first is built using dedicated custom electronics, whereas the second consists in a farm of commercial CPUs running a streamlined version of the CMS offline reconstruction algorithms. During the year-end technical stop occurred between the 2015 and 2016 LHC runs the L1T system underwent a significant upgrade aimed at improving its rate reduction capability in view of the values of instantaneous luminosities expected for the rest of LHC Run-2, which exceed the collider's design specification. As part of this upgrade a new concentrator board, called TwinMux, was introduced. This piece of hardware has the duty to improve reconstruction of trigger segments in the barrel of the muon spectrometer by combining information from neighboring DT and RPC chambers. The logic performed by the TwinMux boards is also simulated by a program, running within the CMS software framework, that is designed to reproduce the hardware behavior. In this thesis the response of the TwinMux hardware and software emulation code is compared using a sample of data collected by CMS during the 2018 LHC run.

Chapter 1

The Compact Muon Solenoid experiment at LHC

1.1 The Large Hadron Collider

The Large Hadron Collider (LHC) is the Hadronic accelerator operating at CERN since 2010 that is placed in a 27 km tunnel, the former LEP tunnel, and capable of accelerating either proton beams or heavy-ion beams. In the first case LHC presently reaches a center-of-mass energy of 13 TeV. The two proton beams run in separate beam pipes and bending, which is needed to make the collisions possible, is achieved using compact twin-bore superconducting magnets, cooled at 2.1 K with superfluid helium, reaching a magnetic field of 8.3 T.

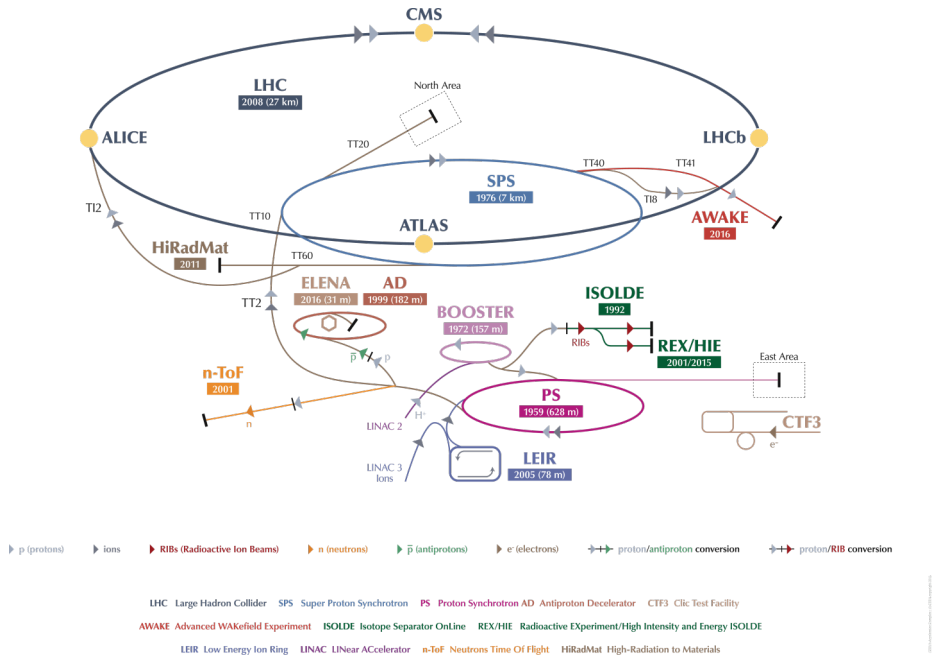

Figure 1.1: The CERN accelerator complex.

The proton injection is done employing pre-existing acclerators. This chain of accelerators, shown in 1.1, comprises the Linac (Linear Accelerator), the PSB (Proton

Synchrotron Booster), the PS (Proton Synchrotron) and the SPS (Super Proton Synchrotron). Given all these steps an injection energy at LHC of 450 GeV is reached. The LHC beam filling requires about two hours. The beam lifetime is about 22 hours, however the data is taken only in the first 10 hours, then the beams are dumped and a new fill is started in order to restart at maximum beam intensity to maximize the integrated luminosity collected by the detectors.

The beams have a bunched structure with a crossing frequency of $f = 40$ MHz, corresponding to a time between collisions of 25 ns, of which an example is shown in 1.2. The bunches contain about $N = 1.1 \times 10^{11}$ protons each.

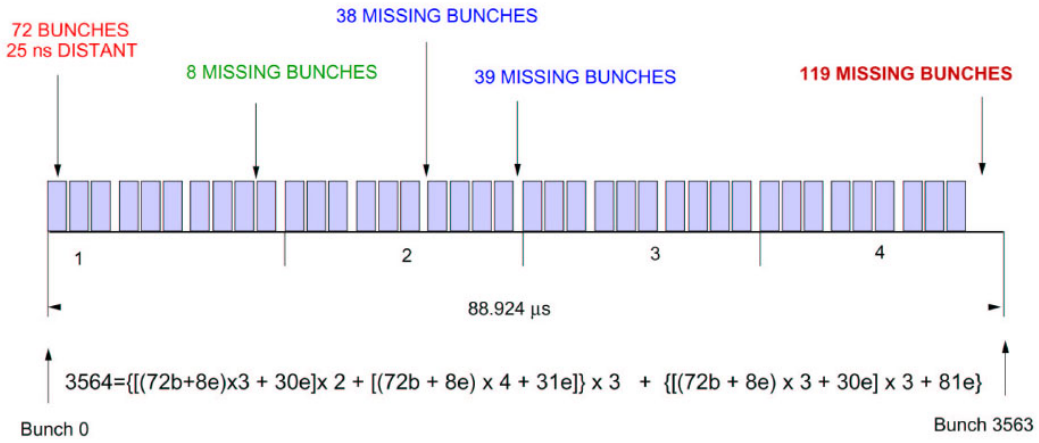

Figure 1.2: The LHC beam structure. It is made up of 39 trains, each one containing 72 bunches. The number of missing packets between a train and the following one allows an absolute synchronization of the electronic systems.

There are four interaction points, where detectors are located: ATLAS (**A** **T**oroidal **L**HC **A**pparatu**S**) and CMS (**C**ompact **M**uon **S**olenoid) are general purpose detectors, ALICE (**A** **L**arge **I**on **C**ollider **E**xperiment) focuses on the heavy ions physics and on the study of the quark-gluon plasma, and LHCb (**LHC** **b**eauty experiment) which study the CP violation in b-physics.

1.2 The Compact Muon Solenoid detector

The Compact Muon Solenoid (CMS) is a general purpose detector 21.6 m long with a diameter of 15 m and a weight of about 12500 tons. It is composed by a cylindrical barrel and two endcaps (1.3).

A superconducting solenoid generates a magnetic field of 3.8 T inside the detector. In its innermost region a high quality central tracking system, capable of achieving a track reconstruction with very high resolution, is installed. A homogeneous electromagnetic calorimeter and a sampling hermetic hadron calorimeter are installed to perform energy measurements on electrons, photons and jets from hadrons. Finally a redundant and highly performant muon system which, provides detection of muon tracks, and contribute to the measurement of their transverse momenta and angular position wraps the detector. Its four muon stations are sliced into an iron yoke that returns the magnetic flux of the

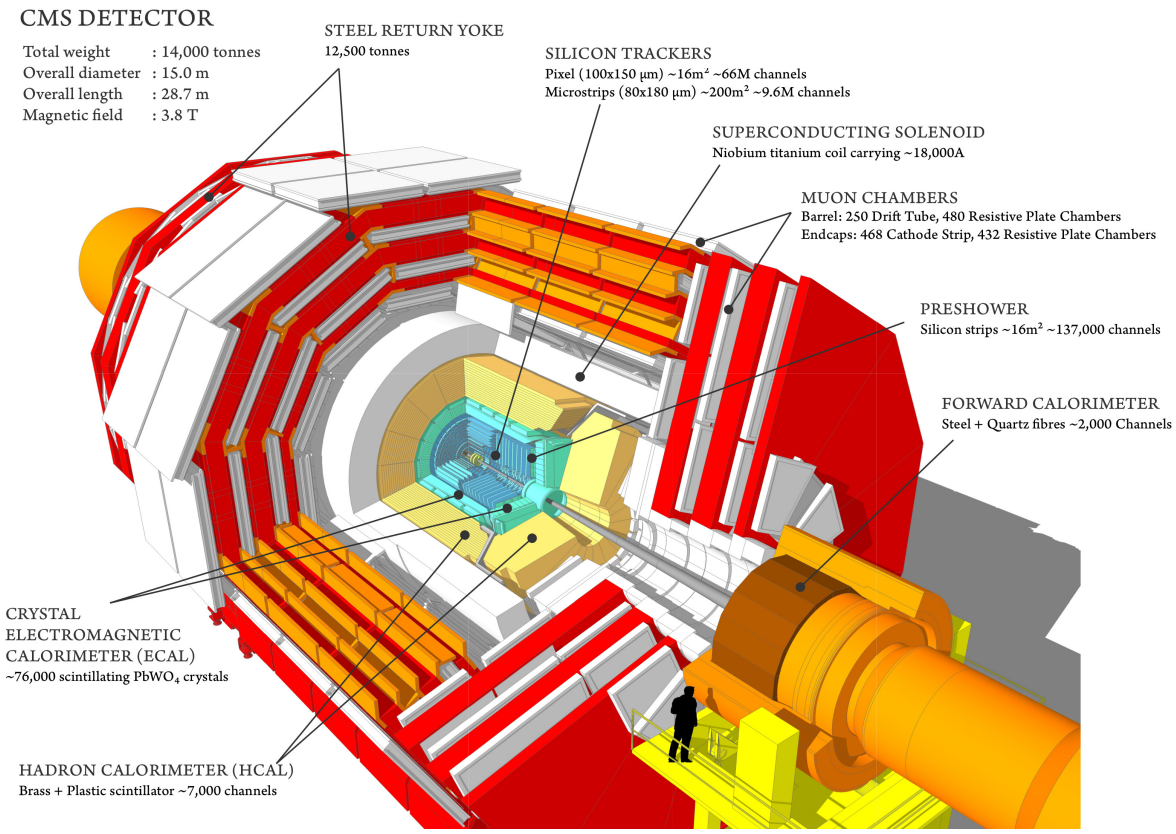

Figure 1.3: Overall view of the CMS detector.

field, acts as an absorber for the traversing particles and hosts and mechanically supports the stations.

In CMS a right-handed coordinate system is defined: the x-axis points to the center of the accelerator ring, the y-axis points upwards and the z-axis is parallel to the beam pipe and the solenoid magnetic field. Beside these coordinates, two angles are defined: the polar angle θ with respect to the z-axis and the azimutal angle ϕ with respect to the y-axis (1.4).

An ultra-relativistic approximation ($|\vec{p}| \gg m$) of the rapidity y, known as pseudorapidity η, is also introduced to replace in most cases the polar angle:

$$y = 1/2 \ln\left(\frac{E + p_z}{E - p_z}\right) \approx \eta = 1/2 \ln\left(\frac{|\vec{p}| + p_z}{|\vec{p}| + p_z}\right) = -\ln\left(\tan\frac{\theta}{2}\right) \tag{1.1}$$

where E, $|\vec{p}|$ and p_z are the energy, the 3-momentum and the component along the z-axis of a particle.

1.3 CMS Muon Detectors

The aim of the muon system is to provide a robust trigger, capable to perform bunch-crossing (BX) assignment and standalone transverse momentum (p_T) measurement, perform efficient identification of muons and contribute to the measurement of the p_T of muons with energy high as few hundreds of GeV and more. The system is the outermost

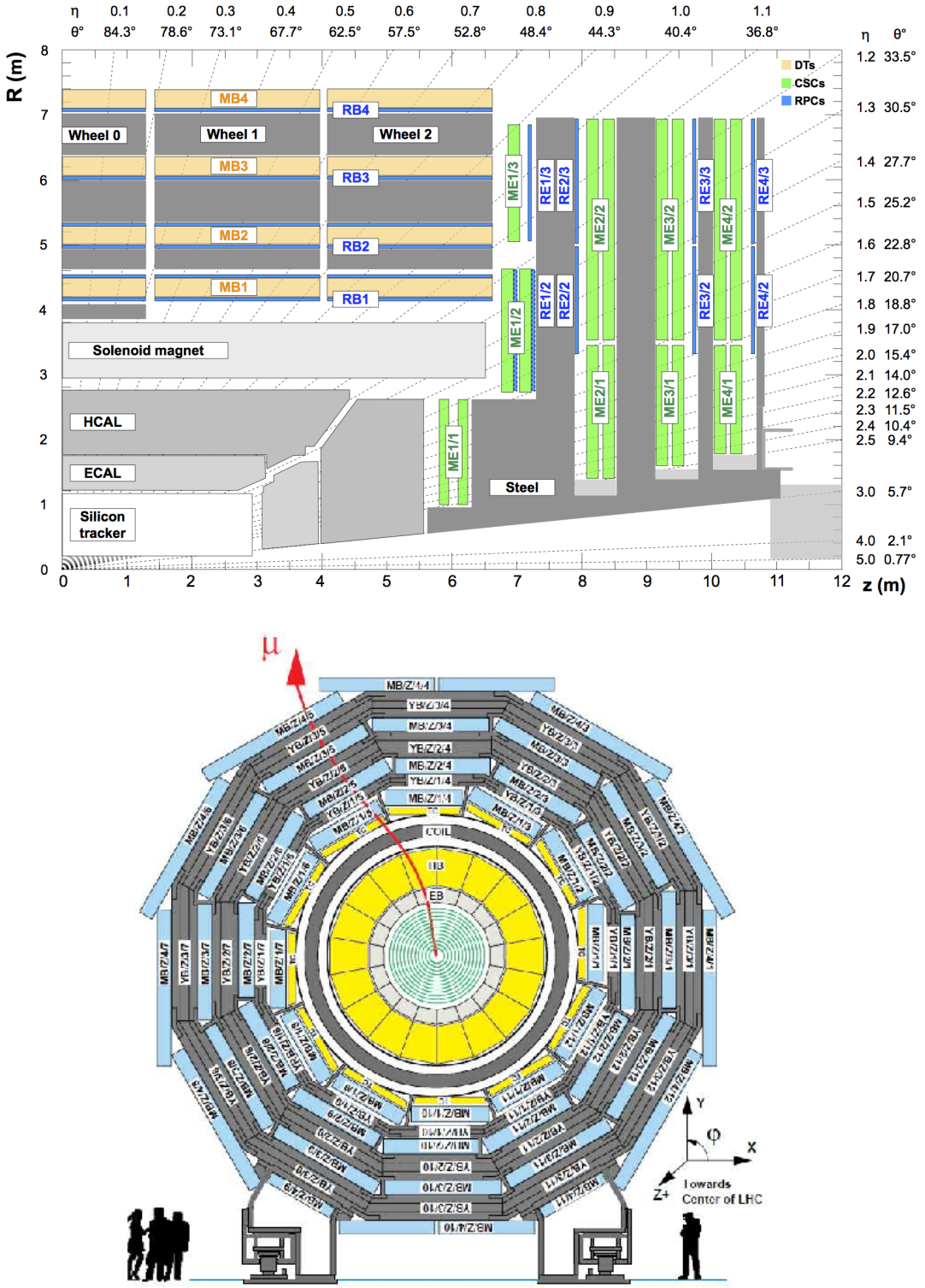

Figure 1.4: CMS detector transverse (top) and longitudinal (bottom) views. Describing LHC a reference frame is usually used in which the x-axis is pointed towards the center of the circular accelerator, the y-axis goes upward and the z-axis runs along the accelerated beam.

detector in CMS: it is embedded in the return yoke of the magnet, allowing the bending given by the magnetic field inside it to be used to measure the p_T of muon tracks. This system is made up of three different redundant detectors. Drift Tubes (DT) are installed in the barrel region ($\eta < 1.2$) because of the low occupancy of muons, low background and low residual magnetic field. In the endcap ($0.9 < \eta < 2.4$), where rate and background are higher and the magnetic field is less uniform, Cathode Strip Chamber (CSC) are used. Both detectors provide precise space and time measurement and have good triggering capabilities. In order to achieve high redundancy, Resistive Plate Chambers (RPC) are deployed throughout the central and forward regions ($\eta < 1.8$): they offer a fast response and an excellent time resolution providing an unambiguous bunch-crossing assignment to muons, thus are mainly dedicated for triggering. Even though the RPCs have a lower spatial resolution than DTs and CSCs, they are also used to complement them in the offline reconstruction.

The CMS regions inside the return yoke of the magnet have the lowest particle rate and radiation doses. The DT system is segmented in 5 wheels along the z direction, each about 2.5 m wide and divided into 12 azimuthal sectors, covering $\sim 30°$ each. Drift tubes are arranged in 4 concentric cylinders, called stations, within each wheel, at different distance from the interaction point, and interleaved with the iron of the yoke. Each DT station consists of 12 chambers in each wheel, with the exception of the outermost station MB4, whose top and bottom sectors are equipped of two chambers each, thus yealding a total of 14 chambers in that station. Each DT chamber is azimutally staggered with respect to the preceeding inner one, in order to maximize the geometrical acceptance. The overall CMS detector is thus equipped with a total of 250 DT chambers.

In the endcap regions of CMS the muon rates and background levels are higher, and the magnetic field is strong and non-uniform. Here, 540 Cathode Strip Chmabers are installed since they have fast response time, they can be finely segmented, and they can tolerate the non-uniformity of the magnetic field. The CSCs cover the η region from 0.9 to 2.4. Each endcap has 4 disks, called stations, of 18 or 36 trapezoidal CSC chambers subdivided in 2 rings, except for the innermost station which is made up of 3 rings, mounted on the faces of the endcap steel disks perpendicular to the beam and interleaved with the iron of the magnet return yoke.

Along the barrel region 480 RPC chambers are distributed in a way similar to the DTs, with two RPC layers for each DT station for the two innermost one, and a single layer for the outermost two. In the endcaps 576 RPC chambers are installed. In the region they cover one single layer of RPCs is interleaved with a single CSC layer.

1.3.1 The Resistive Plate Chambers

RPC have a time response comparable to scintillators, and, with a sufficient high segmentation, they can measure the muon momentum at the trigger time and provide an unambiguous assignment of the bunch-crossing.

A RPC is formed by two planes of material with high resistivity (Bakelite) separated by a 2mm gap filled with a mixture freon ($C_2H_2F_4$) and isobutane ($i - C_4H_{10}$). The planes are externally coated with graphite, which forms the cathode for the high voltage (9.5 kV). The crossing particle generates an electron avalanche which induces a signal in the insulated aluminium strips placed outside the graphite cathodes ready to be read-out. CMS uses double-gap RPCs, with two gas-gap read-out by a single set of strips

in the middle: this increase the signal on the read out strip, which sees the sum of the single gap signals. The readout is segmented into rectangular strips 1-4 cm wide and 30-130 cm long.

1.3.2 The Drift Tube Chambers

The Drift Tubes (DT) are used for the barrel of the CMS muon system because of the large dimension of the surface to be covered.

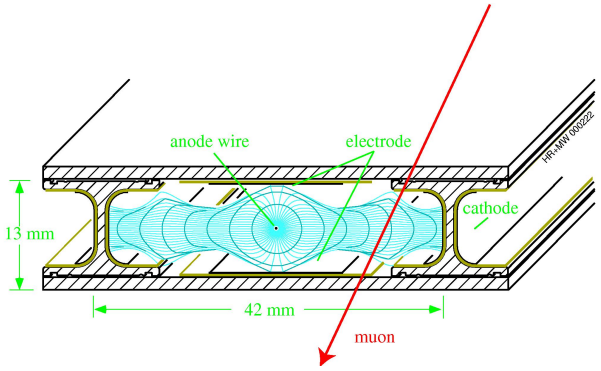

Figure 1.5: The layout of a Drift Tube.

The basic detector element of the DT muon system is a drift tube cell (1.5) of 42 mm $\times$ 13 mm and it contains a stainless steel anode wire with a diameter of 50 μm and lenght varying from 2 to 3 m. Each one of these cells are placed next to each other separated by "I"-shaped aluminium beams, making up layers contained in between two parallel aluminium planes. Strips of aluminium, deposited on both faces of each I-beam and electrically isolated serve as cathodes. Anode wires and cathodes are put at positive and negative voltage (+3600 V, -1200 V) respectively, and provide the electric field within the cell volume. The distance of the traversing track to the wire is measured by the drift time of ionization electrons; for this purpose, two additional positively-biased strips are mounted on the aluminium planes on both inner surfaces in the center of the cell itself, in order to provide additional field shaping to improve the space-to-distance linearity over the cell. The tubes are filled with a 85%/15% gas mixture of Ar/CO_2, which provides good quenching properties. The drift speed obtained is about 55μm/ns. Thus, a maximum drift time (half-cell drift distance) of $\sim$ 380 ns (or 15-16 BX) is obtained.

DT layers are stacked, half-staggered, in groups of 4 to form superlayers. A DT chamber is made up of three superlayers, two of them measure the muon position in the bending plane ϕ, the other one measures the position in the longitudinal plane θ. However, the chambers in the outermost station MB4 have only the two ϕ superlayers.

1.3.3 The Cathode Strip Chambers

Cathode Strip Chambers are multi wire proportional chambers with segmented cathodes, capable of providing precise spatial and timing information, even in presence of large inhomogeneous magnetic field and high particles rates. A charged particle crossing the layers produces a signal which is collected by several adjacent cathode strips; since the strips are deployed radially, a charge interpolation provides a high resolution

measurement of the ϕ-coordinate. The additional analysis of the wire signal offers the measurement of the orthogonal r-coordinate. Wire signals provide a fast response, useful for trigger purposes. Groups of 6 active gas layers form a CSC chamber, with a maximum dimension of $\approx 3.5 \times 1.5 m^2$.

A CSC consist of 6 layers, each of which measures the muon position in 2 coordinates. The cathode strips run radially outward and provide a precision measurement in the r-ϕ bending plane. The wires provide a coarse measurement in the radial direction.

Chapter 2

The CMS Barrel Muon trigger

The task of the trigger system is to perform an online selection of collision events, to reduce the 40 MHz collision rate provided by LHC to the offline storage rate, approximately 1 kHz. The selection criteria is driven by the experiment's physics goals, thus the trigger system must be able to reconstruct physics objects (muons, electrons, gammas, jets, missing energy, etc) with sufficient efficiency and purity to achieve the required rate reduction without compromising the yeld of interesting events. This bandwidth reduction is performed in two main steps, as shown in 2.1. The Level-1 trigger (L1T) is based on custom electronics, and has to reduce the number of accepted events down to a maximum rate of 100 kHz. The High Level trigger (HLT) is based on software algorithms running on a farm of commercial CPUs. At this stage each event can take much more time for its processing, since the bandwidth has been already reduced and events are processed in parallel by different machines of the HLT.

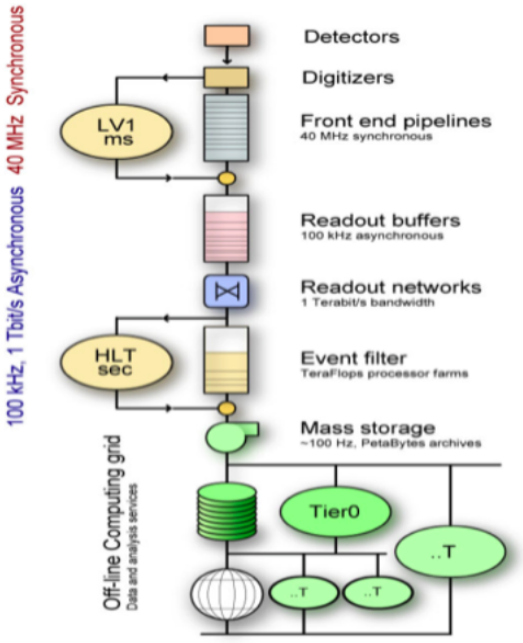

Figure 2.1: CMS trigger bandwidth.

2.1 The Level-1 trigger

The Level-1 trigger must cope with the machine frequency of 40 MHz and the time between collisions, 25 ns, is far too short for running any kind of non trivial algorithm and for taking a decision on accepting that event. However, since dead time has to be avoided, complete information from the subdetectors is stored in First In First Out (FIFO) memories. In parallel, the trigger logic runs using a subset of the information, pipelined in small steps requiring less than 25 ns each, in order to start a new event processing every BX, even if the full processing requires a much longer time to complete. At the end of the logic chain a decision is taken. If the event has to be kept, the FIFO memories containing the detector data are read and sent to the HLT. The maximum time available for the trigger logic to take a decision is determined by the amount of BXs for which the detector data can be stored into FIFOs, and corresponds to 3.2μs.

2.1.1 The L1 muon trigger upgrade

After a shutdown period lasted from 2013 throughout 2014 a second period (Run-II) of data taking started at the beginning of 2015. During this period LHC operated at a center of mass energy of 13 TeV and the average number of interactions per collisions and the instantaneous luminosity have reached the values of approximately 50 and $1.5\times10^{34}cm^{-2}s^{-1}$ respectively. During the LHC Run-II the Level-1 trigger had to cope with an increase of the total event rate of roughly a factor 6 compared to the limits reached during the first LHC run (Run-I).

In view of this increase in luminosity the L1 trigger chain of CMS underwent considerable improvements. Even the L1 muon trigger, which is the main target of this work, was a subject to enhancements. Originally, it was designed to preserve the complementarity and redundancy of CSC, DT and RPC which were used to build tracks separately, until they were combined in the Global Muon Trigger. The upgrade of the muon trigger aimed at exploiting the redundancy of these three systems earlier in the trigger processing chain in order to obtain a high-performance trigger with higher efficiency and better rate reduction.

Since every additional hit along a muon trajectory further improves the rate rejection and muon momentum measurement, the upgrade goal was to combine muon hits at the input stage to the Muon Track-Building stage rather than at its output. All the hits now contribute to the track whatever sub-system detects them.

As for the Run-I muon trigger the track processing is still segmented in sectors of ϕ and η. The upgrade introduced a regional segmentation that treats muon tracks separately depending on η: it distinguishes a barrel region (low η), an endcap region (high η) and a transition region between them ($|\eta| \sim 1$) called overlap. Such regions result in different triggering algorithms but also in different deployments of hardware processors. The final sorting and ghost track cancellation of muon candidates are handled separately for each of the three regions in η.

2.1.2 The L1 muon trigger chain

As we can see in Fig. 2.2, hits from the CSCs are sent to the Endcap Muon Track Finder (EMTF) and the Overlap Muon Track Finder (OMTF) via a mezzanine on the muon port

card. Endcap RPC hits are sent via the link board to the concentrator pre-processor and fan-out (CPPF) card and barrel RPC hits are sent to the TwinMux concentrator card. DT hits are sent to the TwinMux card via a copper to optical fiber (CuOF) mezzanine. The EMTF receives RPC hits via the CPPF card. In addition to the CSC hits the OMTF receives DT hits and RPC hits via the CPPF and the TwinMux, which also provides DT and RPC hits to the Barrel Muon Track Finder (BMTF). The μGMT sorts the muons, performs duplicate removal, adds isolation information from the calorimeter trigger and sends the best eight muons to the Global Trigger.

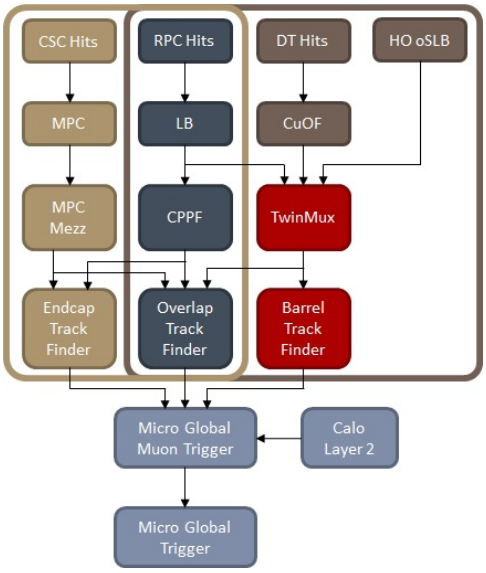

Figure 2.2: Block diagram of the L1 muon trigger. It's visible the geographical concept of this layout.

2.2 The TwinMux Barrel Concentrator Board

The TwinMux is the adaptive layer for the track finder in the barrel region. It merges and transmit information from DT, RPC and Hadronic calorimeter Outer barrel trigger primitives, unburdening the trigger processors. TwinMux is in charge of sending such combined primitive to the BMTF. In both cases a scale up in the transmission rate, and hence a reduction in the number of links, is provided. TwinMux is also responsible for duplicating the trigger primitives in order to reduce connections between trigger processors increasing the reliability of the system. In the barrel region the combined primitives are sent to the BMTF that implements the legacy trigger algorithm of the DT track finder with the addition of several improvements in rate reduction at higher efficiency and quality. For instance BMTF implements an extension of the Run-I algorithm for the p_T assignment that using the primitive bending angle, obtains a factor 1.5 reduction in rate for typical thresholds and the same efficiency at plateau for prompt muons.

2.2.1 The L1 trigger chain in the barrel region

Both TwinMux and BMTF are single slot double-width and full-height μTCA (Micro Telecommunications Computing Architecture) board base around a Virex-7 FPGA (Field Programmable Gate Array) and embedding the optics for high speed data transmission (up to 13 Gbps). The BMTF board is a MP7 card (multipurpose hardware widely used in the trigger update of CMS) while for the TwinMux a custom hardware development was necessary since the DT on-detector electronics transmit data at a low rate requiring a deserialization done by the standard I/O of the FPGA.

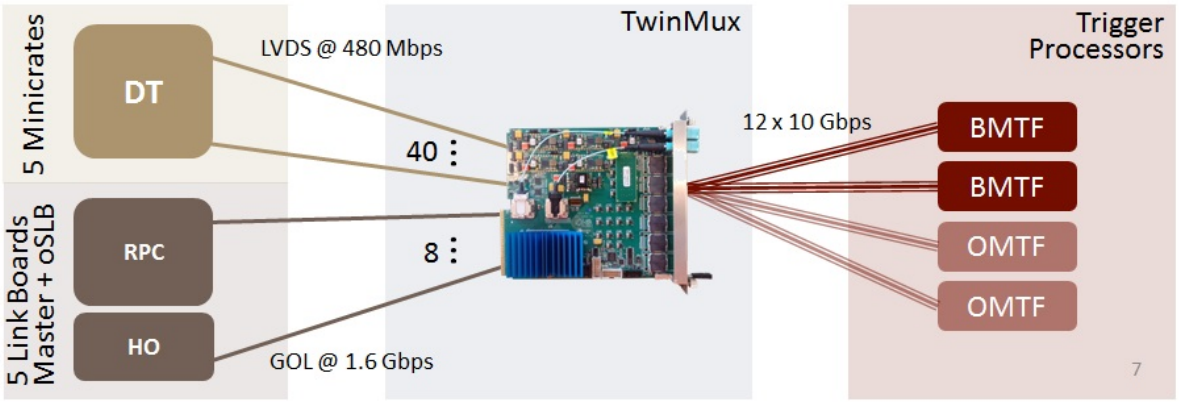

Figure 2.3: DT and RPC trigger chain. TwinMux collects optical links at different rates and merges and fans out data to barrel and overlap trigger processors through high speed links.

From each DT minicrate, the Server Board (SB) transmits the DT trigger primitive over 8 LVDS (Low-voltage differential signaling) links (these links are optically converted by CuOF boards). For the RPC detector five Link Board Masters (LBMs) compress the trigger hit data relative to one 30° sector and serialize it through the GOL transmitters. TwinMux is in charge of forwarding this data to the BMTF and to the OMTF applying a scale up in the transmission rate (and hence a reduction in the number of links). TwinMux is also responsible for duplicating (up to four times for the sectors of the outer wheels where data are shared between barrel and overlab track finders) in order to reduce connections between trigger processors increasing the reliability of the system. The minimum bandwidth required for forwarding trigger data of one sector is 16 Gbps for DT data and 8 Gbps for the RPC which needs a total of three high speed links.

2.2.2 The TwinMux architecture

TwinMux is a single slot double-width full-height μTCA board, equipped with 6 front panel SNAP12 receivers and 2 Minipods (one transmitter and one receiver) for high speed data transmission (up to 13 Gbps). Based around a Xilinix Virex-7 FPGA, the TwinMux achieves the merging of several 480 Mb/s trigger links to higher speed serial links and compensates delays to provide BX alignment of the trigger data coming from different inputs.

The clock distribution is based on two very low jitter PLLs (Phase-Locked Loops) that can broadcast to all the FPGA's transceivers two different clocks for performing

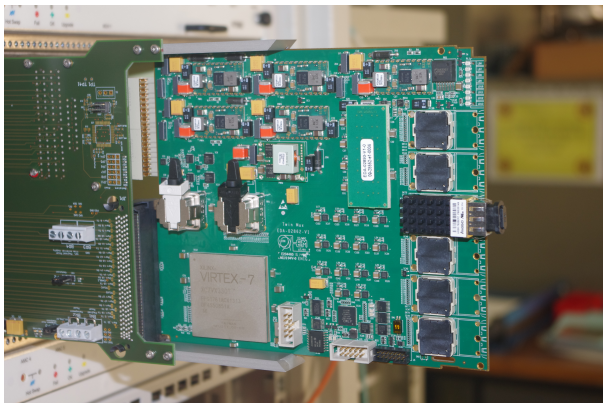

Figure 2.4: The TwinMux board.

synchronous or asynchronous data transmission. Finally a microcontroller is responsible for managing the IPMI (Intelligent Platform Management Interface) on the backplane that handles low level operations like hot-swap or temperature sensors monitoring.

To cover the full barrel, 60 TwinMux are hosted in 5 μTCA dual star crates, each of which is equipped with an AMC13 for clock and slow control commands distribution and for providing a connection to central DAQ. Each crate is also equipped with a commercial μTCA Carrier Hub (MCH), a redundant power module and a JTAG switch used for programming remotely each TwinMux board.

2.3 The TwinMux Algorithm

The TwinMux hosts an algorithm aimed at improving the trigger performance through the simultaneous use of DT and RPC information. This is achieved through two main operations: the calculation of DT+RPC primitives, called Super Primitives, and of RPC-only primitives. Each TwinMux processor receives DT and RPC links from one sector of the barrel muon detector. The data coming from these two detectors contains different informations. Trigger Primitives are sent from DTs and they include position, direction, quality and BX information. On the other hand Hits coming from RPCs include position and BX information only. However output data to the BMTF use the same data format as the DT Trigger Primitives.

The DT+RPC primitives are obtained following an algorithm which has several steps. First, input data are deserialized and synchronized. Then a clustering algorithm is applied to RPC hits: neighbouring hits are merged and the resulting cluster position is assigned with half-strip resolution and converted into DT coordinates. In case that the same RPC cluster fires in two consecutive BXs, the second one is suppressed. RPC clusters close in ϕ to DT Trigger Primitives from the same chamber are then searched for in a $\pm$ 1BX time window centered around the DT primitive BX. After that the closest RPC cluster is selected and if the $\Delta\phi$ with respect to the Trigger Primitive is equal or less than 15 mrad, RPC and DT are considered matched and a DT+RPC primitive quality flag is set. Furthermore, if the DT Trigger Primitive was built with less than 8 DT ϕ layers, the Trigger Primitive BX is shifted to match the RPC cluster BX; if it was built with all 8 DT ϕ layers, its BX is not changed. Whenever no match with an RPC cluster is found, the original DT Trigger Primitive is sent to the BMTF and

the DT+RPC primitive quality flag is not set. In MB1 or MB2 station, if there is no DT primitive available, "pseudo primitives" can be built. In fact, MB1 and MB2 are equipped with two RPC chambers, installed on the two opposite sides of the DTs with respect to the beam line. If RPC clusters from these two chambers are close in space, they are combined and position and direction are computed and used to create an additional primitive which is sent to the BMTF, potentially increasing the number of station layers used to build a BMTF track. An emulator by the research group from University of Ioannina was developed in order study the TwinMux performance in the design stage of the trigger upgrade. This emulator is not a bit-wise emulation of the hardware, nevertheless it has been deemed accurate enough to simulate the hardware response during the production of Montecarlo samples [6].

2.3.1 Efficiency improvements

Thanks to the superior timing capability of the RPC detectors, the DT+RPC barrel trigger primitive has a better BX identification than the DT-only trigger primitive, that translates in an improved trigger efficiency. This is shown in Fig. 2.5, where the efficiencies of DT and DT+RPC trigger primitives in MB1 are plotted versus the pseudorapidity. The average efficiency gain with the introduction of DT+RPC was $\approx 1.4\%$.

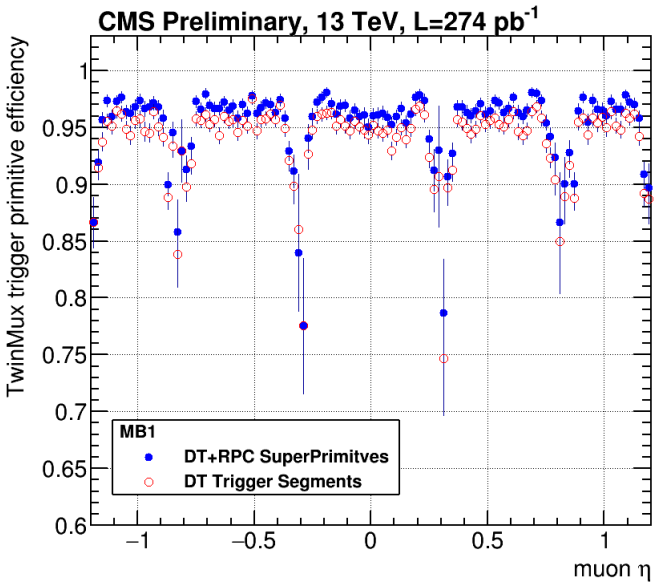

Figure 2.5: Trigger Primitive efficiency, for the MB1 station, versus the reconstructed muon pseudorapidity η . In red, open circles, the efficiency of DT-only Trigger Primitives. In blue, solid circles, the efficiency of DT+RPC primitives. An average increase of the efficiency of about 1.4% is observed: from 94.1% (DT Local Trigger) to 95.5% (DT+RPC primitives)

The RPC-only trigger primitives are particularly useful in case of problems affecting the DT detector, ensuring triggers are generated even in case of complete lack of input from a DT chamber. Nevertheless, there is an increase in overall efficiency even in standard, healthy detector conditions, as shown in Fig. 2.6, where the efficiency for

DT-only and DT+RPC primitives (red open circles) is complemented with the inclusion of RPC-only primitives as well (blue full circles) [2].

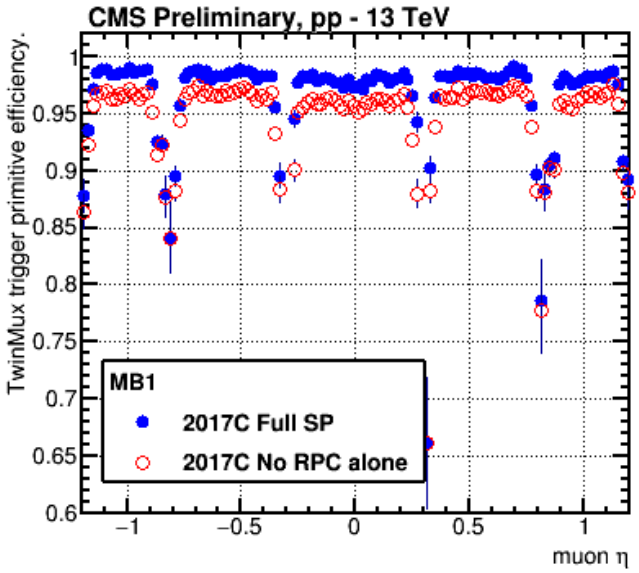

Figure 2.6: Trigger Primitive efficiency, for the MB1 station, versus the reconstructed muon pseudorapidity η. In red, open circles, the efficiency without the introduction of RPC-only primitives. In blue, solid circles, the efficiency with all the primitives types included.

This gain in overall trigger primitive effciency has positive effects downstream in the trigger algorithm: the Barrel Muon Track Finder is fed, in average, with more track segment per muon. This translates into not only in an increase of BMTF tracking effciency (Fig 2.7) , given that the algorithm requires at least two track segments to build a L1 muon track, but also in a reduction of the trigger rates. In fact, the availability of more segments along the muon trajectory allows a slightly improved momentum estimate. With no drawbacks at high luminosity, the inclusion of the RPC-only segments reduced the trigger rate for barrel muons with $p_T > 25$ GeV by 3%, by improving the BMTF p_T assignment [3].

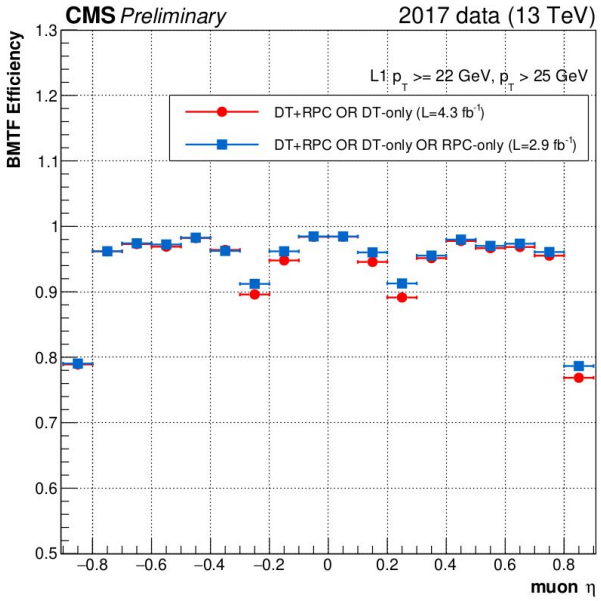

Figure 2.7: BMTF efficiency versus the reconstructed muon pseudorapidity η. In red the BMTF efficiency with DT+RPC and DT-only primitives; in blue, the efficiency adding the RPC-only primitives. By adding redundancy to the algorithm, up to 2% higher efficiency is observed in the crack regions (space in between wheels around $|\eta| \approx 0.25$ and $|\eta| \approx 0.85$).

Chapter 3

Comparison between TwinMux and Emulator Data

The algorithm implemented in the TwinMux hardware is simulated within the CMS software by an emulator, developed by researchers of the University of Ioannina. The goal of this analysis is to evaluate the capability of the simulation to reproduce the behavior of the hardware, by comparing the results of the emulator with the actual data from the TwinMux. As said in 2.3, the present code is not intended to perform a bit-wise emulation of the hardware, anyhow, as a matter of simplicity, we will refer to the TwinMux simulation code as the emulator. As a result of this limitation, the emulator cannot be compared with the hardware output on a bit-by-bit basis and a little more insight is needed to make the performed studies meaningful. One can, for example, validate that, in a statistical sense, its response is accurate enough to satisfy the needs of montecarlo simulations. Moreover it is possible to pinpoint the cases were discrepancies arise, in order to drive the development of a more accurate code. In this work, we have compared quantities linked directly to the creation of primitives, such as counting how many of them are built, which BX is associated to them in data and by the emulation, and how accurate the local position and direction assigned by the trigger for RPC-only primitives is, compared to the offline reconstruction. Most of the results we have obtained indicate that, though a "fair" agreement in terms of overall performance is reached, there is margin to improve the simulation of the TwinMux algorithm.

3.1 Dataset

The data used for this analysis collected by the CMS detector during the proton-proton running at $\sqrt{s} = 13$ TeV of the Large Hadron Collider at the beginning of September 2018, and it corresponds to around 400 pb^{-1} of integrated luminosity. After being stored, data was further processed with the CMS offline software to perform reconstruction of physics objects. In particular track segments were built within single DT chambers. A further event selection requires pairs of oppositely charged muons with an invariant mass above 60 GeV (the algorithm used for this skimming is consultable at [8]). The resulting dataset has been further processed locally, to add the information produced by the TwinMux emulator, and saved in a flat ROOT [9] tree format for easier analysis.

At this point, the data available for this analysis contained 393288 events, mostly from

Drell-Yan $\rightarrow \mu\mu$ decays, and included the following information, which was relevant for this study: first of all DT trigger primitives as read out from the TwinMux board input buffers, then Barrel Trigger Primitives as read out from the TwinMux board output buffers and as produced by the TwinMux emulator software, and finally track segments, reconstructed at the level of individual DT chambers by the CMS offline software, built with DT hits read out at full precision. This last type of object, given its superior spatial resolution, has been useful to evaluate the position and angle measurement provided by the newly introduced RPC-only trigger primitives.

3.2 Analysis Strategy

To reduce ambiguities and to isolate well defined features of the algorithm, the data has been divided into two classes aimed at investigating separately the properties of RPC-only primitives and of DT+RPC primitives which resulted in a change of the BX with respect to the one assigned by the DTs. Events containing RPC-only primitives, discussed in 3.4, are selected looking for TwinMux output primitives with no DT primitives available at TwinMux input. Events with a BX change were selected requiring a single DT input and a single TwinMux output with a different BX. This case is looked into in 3.5.

Before the comparison of the specific cases described above, we have analyzed the dataset in our possession inclusively to establish the fraction of times in which the TwinMux complements DT primitives with RPC information.

3.3 Trigger Primitive Quality

The DT Trigger primitives received from the TwinMux include quality information. The quality is an integer value, which can vary from 2 to 6, that describes the number of layers from a DT chamber involved in the creation of the primitive. If this flag is set to 2 or 3 (High In and High Out) it means that only one superlayer of the two contained in a chamber is used, respectively the innermost or the outermost one. In this case, primitives must be built using all the 4 layers of a superlayer. The number 4 (LL) refers to the case where both superlayers are used but a trigger primitive is built using 3 layers out of four from each superlayer. Numbers 5 (HL) and 6 (HH) correspond respectively to: a primitive built with 4 DT layers from one superlayer and 3 from the other; a primitive which is built using all the eight layers in a DT chamber. Fig. 3.1 shows how the primitives with different qualities are treated by the TwinMux (left) and by the emulator (right).

The different colors in the histograms represent: i. the number of times in which RPC-only primitives are generated by the TwinMux algorithm (violet); ii. the ones where RPC information is used to perform a BX assignment correction to an existing DT primitive (green) and iii. the number of times were no explicit use of the RPC information is made (beige). The plots are computed considering only the cases when a single TwinMux primitive is present in a given chamber for the hardware and the emulator respectively. The cases in which a BX correction happens are, in general, more frequent for lower quality triggers. The plot also shows that no BX correction is

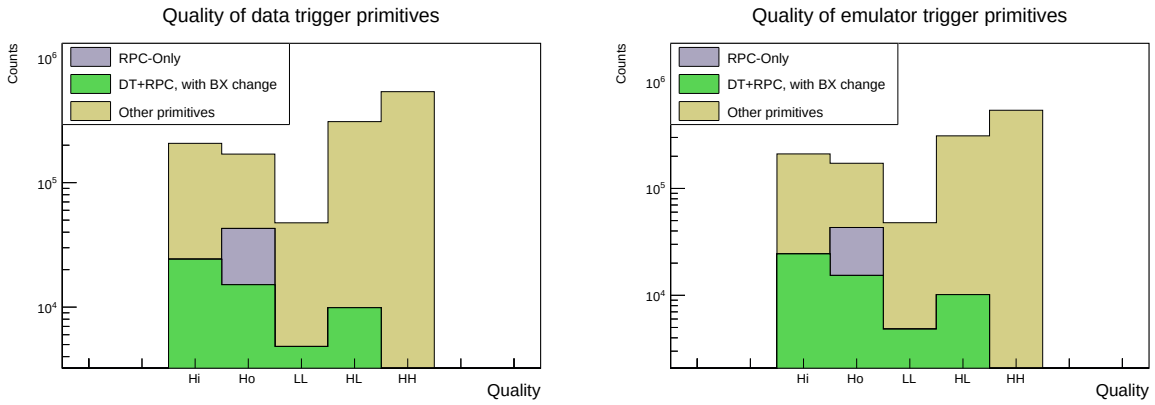

Figure 3.1: Distribution of quality of RPC-Only primitives in violet, DT+RPC primitives with a BX change in green and other primitives in beige, in the TwinMux board output on the left and in the emulator on the right. The plots are computed considering only the cases when a single TwinMux primitive is present in a given chamber.

performed for HH primitives. This is expected as DT primitives with the highest quality are characterized themselves by very accurate BX assignment, hence the TwinMux is configured to avoid any attempt of BX correction based on RPC information in this case. Overall the right and left plots in 3.1 are very similar, showing that the emulator and the hardware perform, in a statistical sense, rather similarly. The fraction of cases in which the TwinMux hardware (emulator) performs a BX correction are 4.25% (4.28%) whereas the fraction of times when an RPC-only primitive is built are 2.18% (2.17%) with respect to a total amount of 1271960 (1279786) primitives.

3.4 RPC-only Primitives

First of all, the TwinMux output primitives with no corresponding input coming from DT chambers were selected among all data coming out the TwinMux board or the emulator. The plots which can be obtained mapping these tracks depending on their location in the barrel of the CMS detector (wheel, sector and station), are slightly different whether the output is from the real hardware or the emulator. No such cases are expected in the third and fourth station, in fact, as described in 2.3, these two stations have only one layer of RPCs, whereas two of them are necessary to build a RPC-only primitive. From the study we confirm that this feature is emulated correctly.

3.4.1 Spatial Distribution of RPC-only Primitives

In order to compare the real and emulated RPC-only primitives, we have checked, in MB1 and MB2, the probability that the two outputs differ in the following way.

First, we select events with a RPC-only primitive in real data. The distribution of such events as a function of sector and wheel is shown in the left-hand side of Fig. 3.2 for the MB1 station (top) and MB2 (bottom). We can see that such objects are produced by all chambers with the exception of two MB2s in YB-1, sectors 4 and 7, which have no entries, and YB-1 sector 4 MB1 and YB2 sector 12 MB1, which have a number of

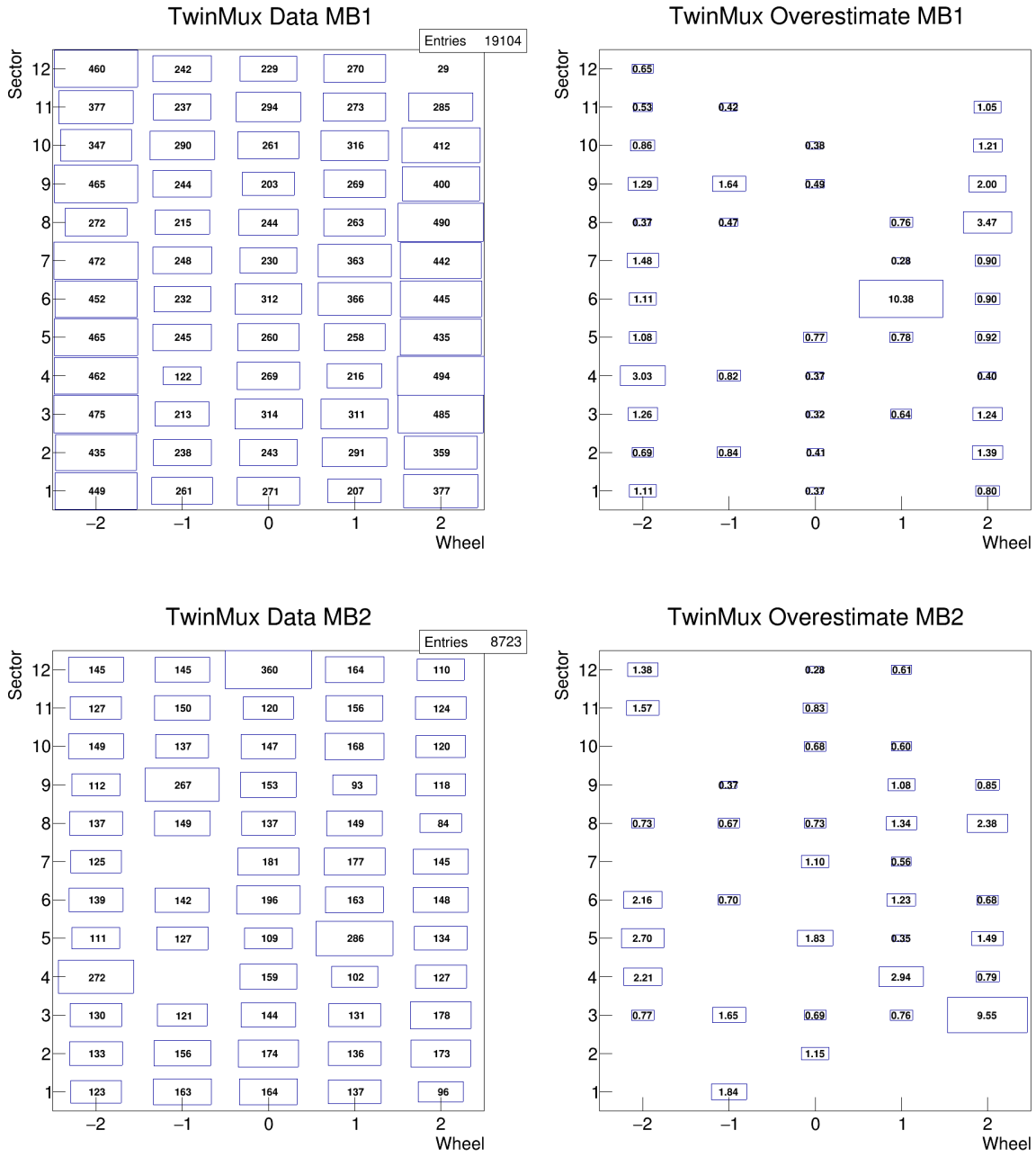

Figure 3.2: Distribution of RPC-only primitives built by the TwinMux in MB1 (top) and MB2 (bottom) as a function of their wheel and sector. On the left side all the primitives are shown. On the right side the percentage of primitives in each wheel and sector not reproduced by the emulator is shown.

entries significantly lower than the neighbouring chambers. This was verified to be due to problems in these RPCs, which were, at least in part, not operational during the data taking. Some chambers show an occupancy significantly larger than the average, instead; an explanation could be that some noisy detector channels results in a larger rate of trigger primitives in some location of the detector. An interesting feature visible in these plots is that the MB1 chambers in YB$\pm$2 have a larger occupancy than the others. This

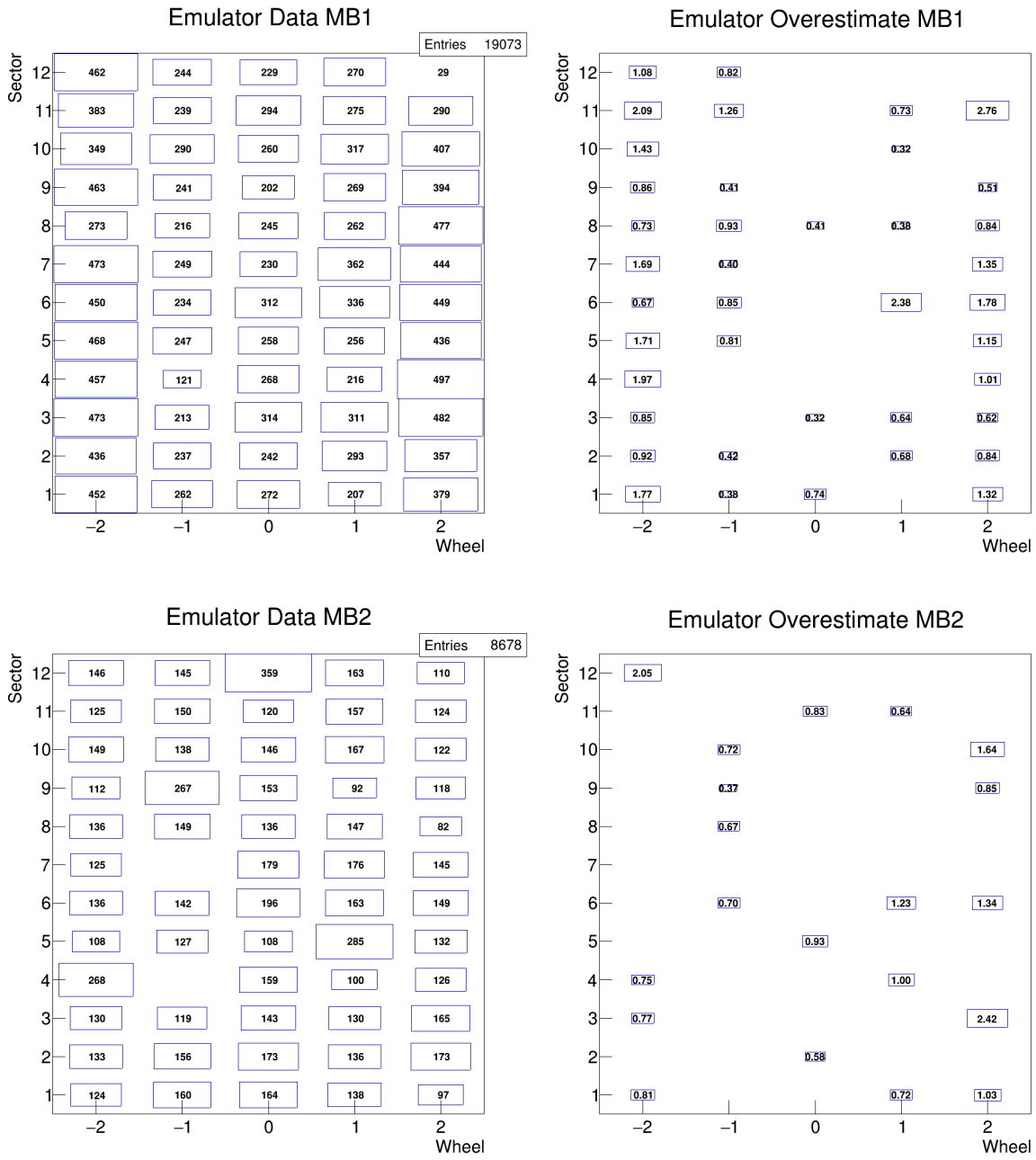

Figure 3.3: Distribution of RPC-only primitives built by the emulator in MB1 (top) and MB2 (bottom) as a function of their wheel and sector. On the left side all the primitives are shown. On the right side the percentage of primitives in each wheel and sector not reproduced by the TwinMux is shown.

is somehow expected, as the overall rate, due to both genuine muons and background, is larger in these chambers being them the most forward ones of the barrel muon detector. On the right side of Fig. 3.2 we show similar maps for MB1 and MB2 stations where we select events requiring that the emulator did not produce the RPC-only primitive that was found in data. These plots are normalized with respect to the previous ones, so that the number within each bin represents the probability (as a percentage) that the

emulator did not deliver the RPC-only found in data for the corresponding chamber. We can see that this happens very rarely, with an average probability of $\sim 0.8\%$ for both MB1 and MB2; nevertheless, the probability seems to be consistently higher in MB1 YB ± 2. This could be due to a difference between the real algorithm and the emulator that is enhanced in the presence of larger hit rate. In addition a couple of chambers, YB1 sector 6 MB1 and YB2 sector 3 MB2, seem charachterized by a larger rate of discrepancy compared to the rest of the detector. Further investigation, required to better clarify this mismatch, that is nevertheless small, and that could be performed focusing on the chambers with larger discrepancy, goes beyond the scope of this work.

The complementary study, performed selecting events where the emulator finds RPC-only primitives, and looking for the lack of a correspondence in the TwinMux data, is shown in Fig. 3.3. The left shows a similar pattern in the distribution of signals in MB1 and MB2, for example the chambers with less occupancy seen in real data are visible also in these plots. On the right side of 3.3, we show, instead, the number of RPC-only which are built by the emulator but not produced by the hardware. The fraction of emulator-only tracks is in average about 0.8% for MB1 and 0.3% for MB2, which are not dissimilar from the case discussed before. Further studies are needed to investigate the discrepancy between the hardware algorithm and the emulator in the creation of the RPC clusters or in their matching. In particular the matching of two RPC clusters, needed to create a RPC-only trigger primitive, depends on a spatial window and the agreement of its definition in hardware and emulation should be cross-checked.

3.4.2 BX-ID Comparison in RPC-only Primitives

Constructing a primitive with only the information coming from RPCs also implies assigning a BX to them. In Fig. 3.4, the BX of the trigger primitives produced by the emulator is shown as a function of the BX of the primitives produced by the TwinMux hardware. For the events where both are found, most occurences are on the diagonal, meaning that the majority of the primitives in the data and in the emulation have the same BX, even though a small percentage (around 0.07%) of all primitives have a different BX assignment in emulation and data.

This comparison has been conducted only in a ± 2 BX window according to the range around the central BX processed by the emulator.

3.4.3 Spatial resolution of RPC-only Primitives

Focusing on primitives built both by the TwinMux and the emulator at the same BX, we can evaluate the resolution of the local position and direction with respect to the primitives reconstructed offline. This test is important as it permits to compare the spatial resolution of RPC-only primitives in data and emulation, and this quantity has an impact on the reconstruction and p_T assignment of L1 muon candidates in the BMTF.

To allow this comparison the trigger quantities were converted to the reference frame used by the offline reconstruction. In fact trigger primitive position is specified as angle, ϕ, that represents the angular position of the primitive with respect to the point where the chamber is perpendicular to a straight line coming from the beam line; the direction is defined as a second angle, called ϕ-bending, that is the angle between the track direction and the ϕ angle. The offline segments, instead, use an orthogonal local reference frame,

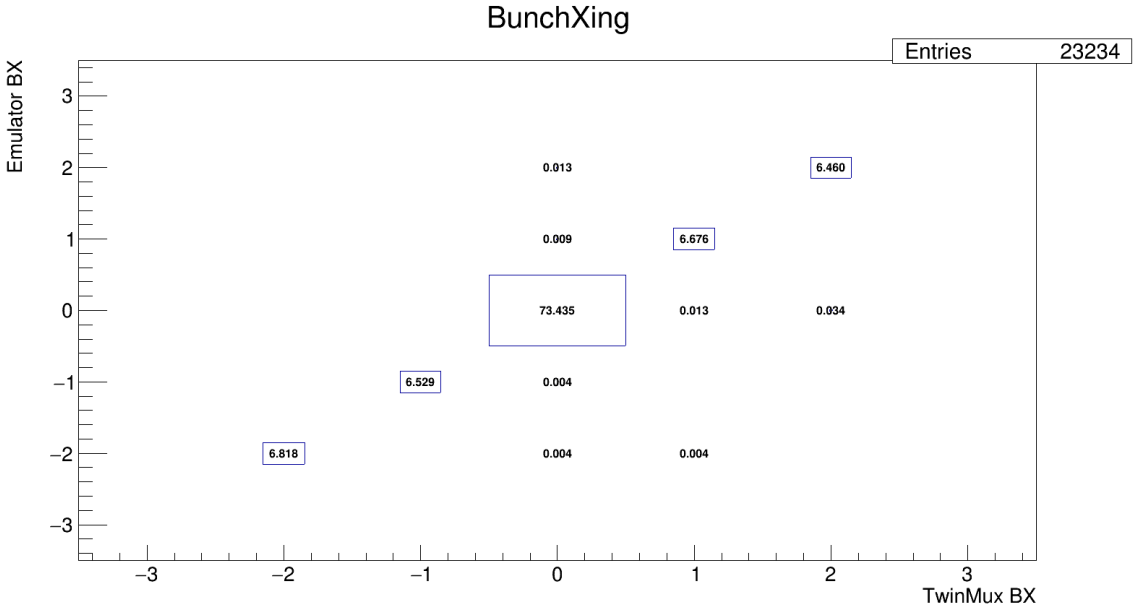

Figure 3.4: One to one comparison of Bunch-Crossing identification between TwinMux and Emulator for RPC-only primitives contained in both outputs. The fraction of primitives with a different BX-ID in data and emulator output is under 0.1%.

centered in the middle point of the chamber and aligned with it. The conversion between the two coordinate systems is performed using a software tool [7] which, as regards the position, calculates the distance from the center of the chamber multiplying its distance along the z-axis with the tangent of ϕ converted in radiants, and for the direction adds the ϕ-bending and ϕ.

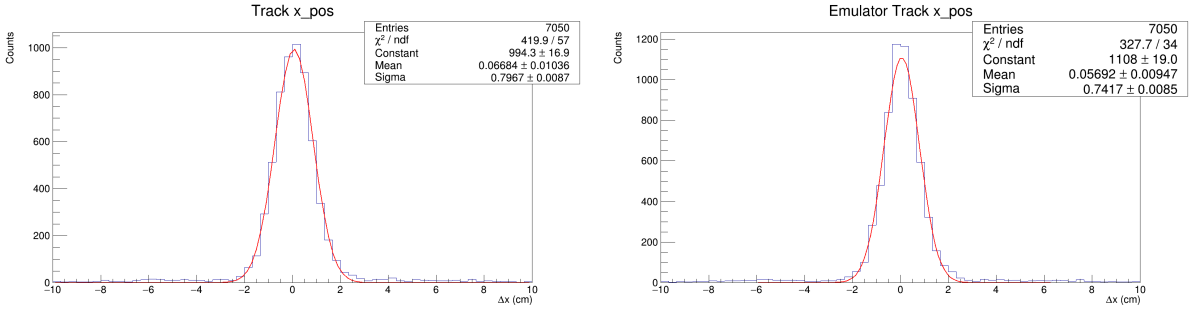

Figure 3.5: Difference between the local position of segments reconstructed offline and the one calculated from the angle information from the TwinMux in data (left) and emulator output (right), then fitted with a gaussian. The peak is in both cases very close to 0, indicating a good grade of agreement between the reference frames of offline and trigger primitives. The width of the curve is in agreement with the expectation from the spatial resolution of RPC cluster used to build the primitives.

The difference between the position, calculated in this way from TwinMux (left) and emulator data (right), and the one in the offline segments information is shown in Fig. 3.5 and it is fitted with a gaussian to acquire the most accurate estimation of mean and

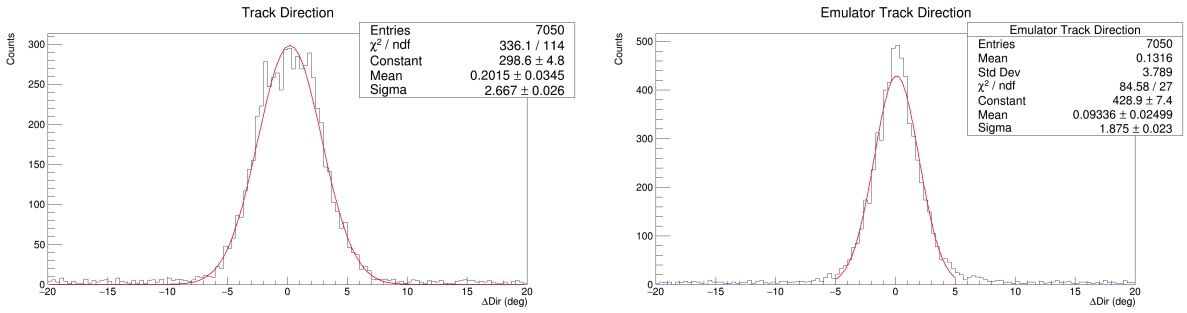

Figure 3.6: Difference between the local direction of segments reconstructed offline and the one calculated from the angle information from the TwinMux in data (left) and emulator output (right), than fitted with a gaussian. Data forms a larger curve then the emulator and the gaussian mean of the latter results closer to 0. However, both data and emulator are in rough agreement with expectations, considering the spatial resolution of RPC clusters used to build the primitives.

standard deviation σ. The means of both distributions are very close to 0, implying that no overall bias is present in the position assignment of the TwinMux hardware or emulator. The width of the curve is also consistent with the resolution expected for clusters of RPC hits which enter the TwinMux. The direction resolution in Fig. 3.6, instead, even though it has a peak near 0 in both cases, has a wider shape, in real data (left plot), if compared to the emulator (right plot), resulting in a greater RMS for the former. This discrepancy, apparently due to a problem affecting only the hardware, will also require a follow up study. A first possible test could be to compute the resolution plot for different chambers independently, to disentangle the possibility that the widening of the RMS is actual due to a convolution of shifts in the mean of the distribution for different chambers.

3.5 DT+RPC Combined Primitives

When a DT trigger primitive is available, the TwinMux evaluates the presence of RPC clusters geometrically matching it, then uses these clusters to improve the accuracy of the BX assignment, as described in 2.3. To perform a data versus emulator comparison of this part of the algorithm, data have been selected requiring exactly one DT trigger primitive and a different BX assigned to the trigger primitives at input and output of the TwinMux. The same selection has been applied to both real data and emulation.

3.5.1 Spatial Distribution of DT+RPC Primitives

An approach similar to the one followed to analyze the RPC-only primitives has been developed. Occupancy maps for MB1 (top) and MB2 (bottom) are shown in the left side of Fig. 3.7 and 3.8, for data and emulator respectively. All chambers seem to be operational and the effect of a larger rate at high pseudorapidities is again visible as an average occupancy in MB1 of YB±2 larger than in the rest of the detector.

The right-hand side of the figures shows the discrepancies between data and emulator,

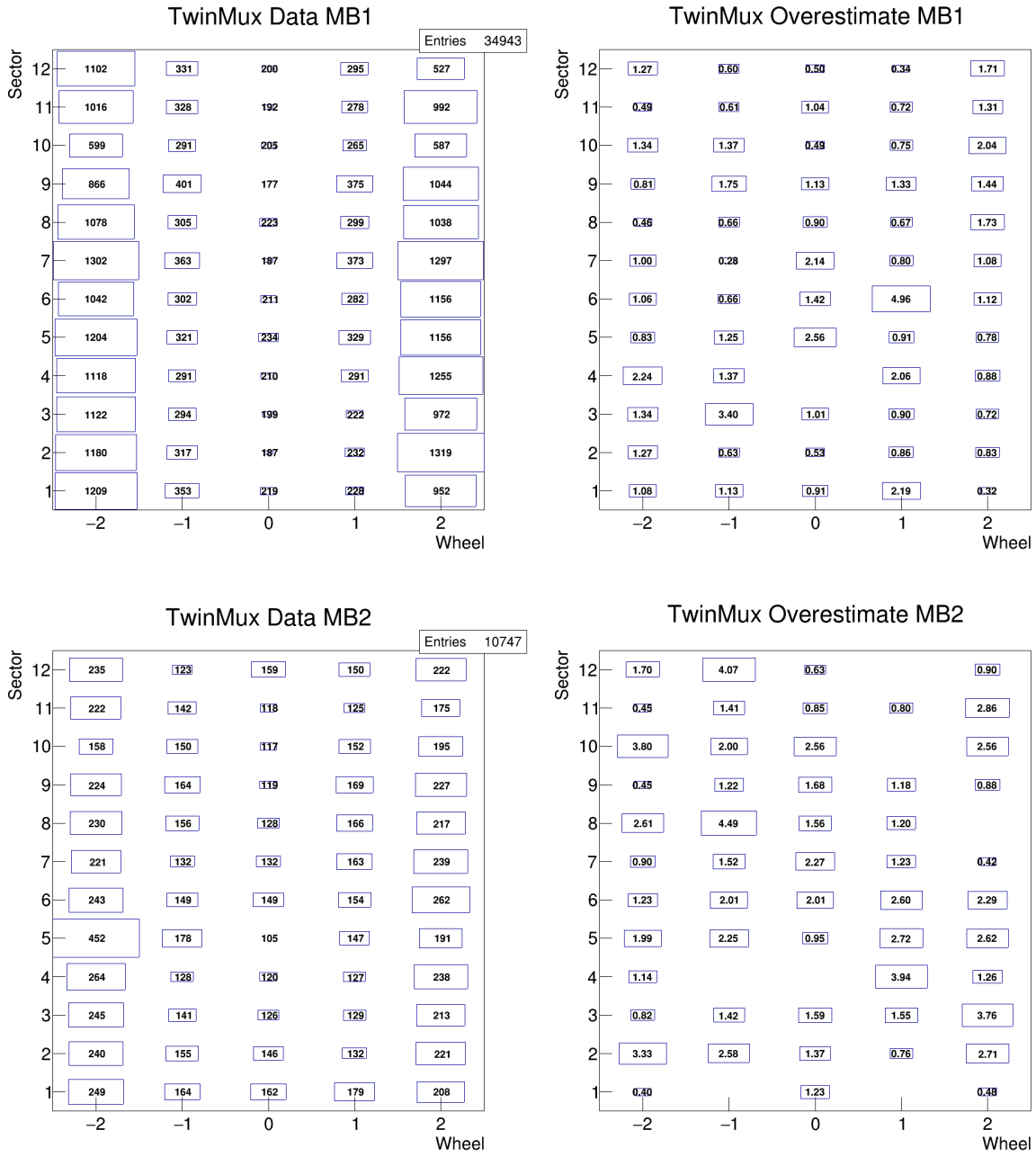

Figure 3.7: Distribution of DT+RPC primitives built by the TwinMux in MB1 (top) and MB2 (bottom) according to their wheel and sector. On the left side there are is the occupancy of the total TwinMux output associated with a single DT input. On the right hand side the percentage of primitives in each wheel and sector where the emulator does not reproduce the hardware behaviour is shown.

in term of data trigger primitives not found in the emulator (Fig. 3.7) and of emulated trigger primitives not found in data (Fig. 3.8). The probability of such occurrences seems to be roughly flat across the detector and it amounts around 1.1% and 2.7%, respectively, in MB1 and 1.6% and 2.3% in MB2.

Since the BX correction is possible using also a single RPC chamber (while two cham-

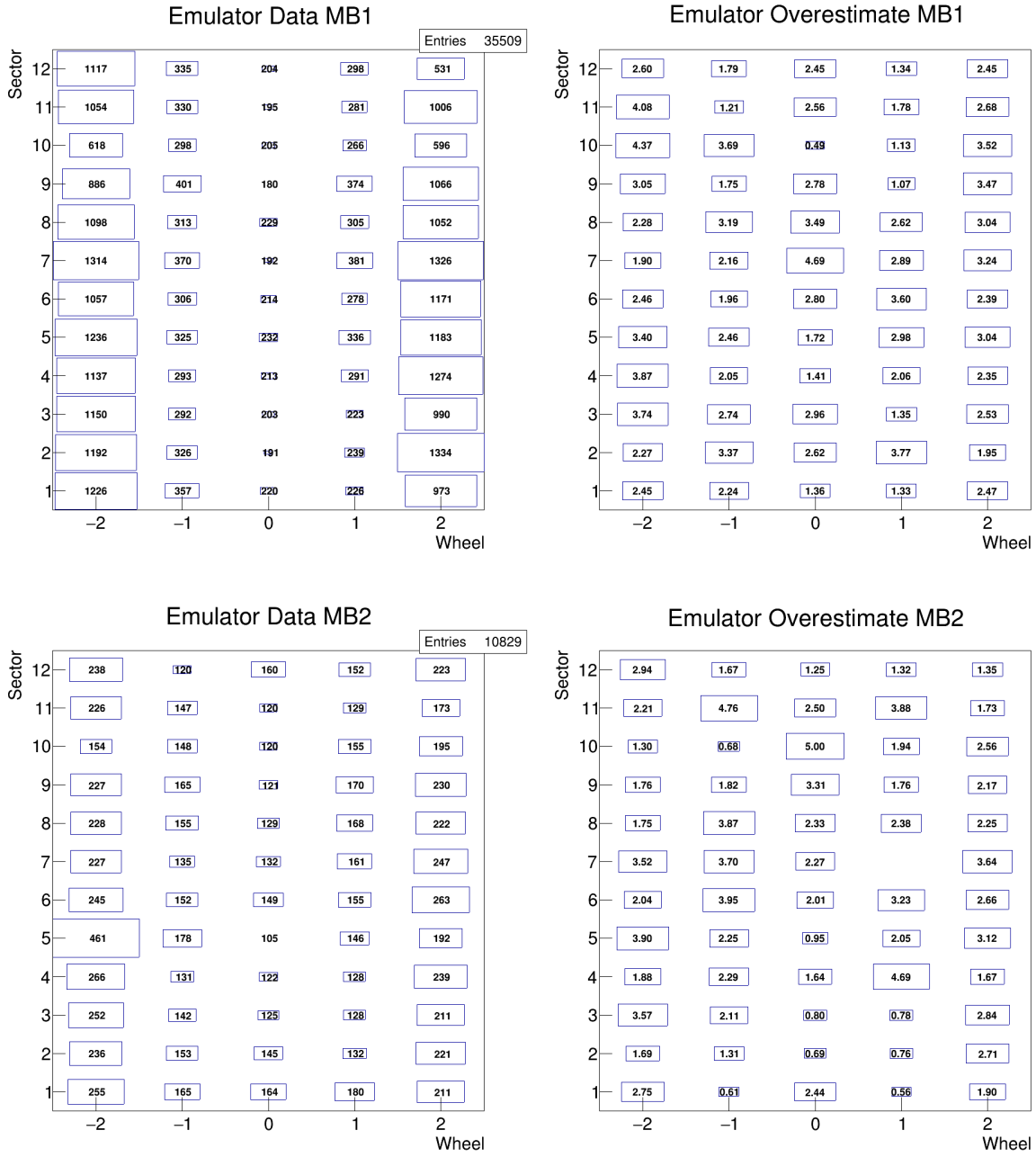

Figure 3.8: Distribution of RPC+DT primitives built by the emulator in MB1 (top) and MB2 (bottom) according to their wheel and sector. On the left side there are is the occupancy of the total emulator output associated with a single DT input. On the right hand side the percentage of primitives in each wheel and sector where the emulator does not reproduce the hardware behaviour is shown.

bers are needed to build RPC-only primitive, discussed in 3.4), we report similar maps also fot the MB3 and MB4 stations in Fig. 3.9 and Fig. 3.10. The statistics available in these stations is lower and it is difficult to exclude any feature in the geographical distribution of the mismatches; nevertheless, the average mismatch probabilities amount to 1.5 % and 1.02% in MB3 and 2.4% and 2.0% in MB4.

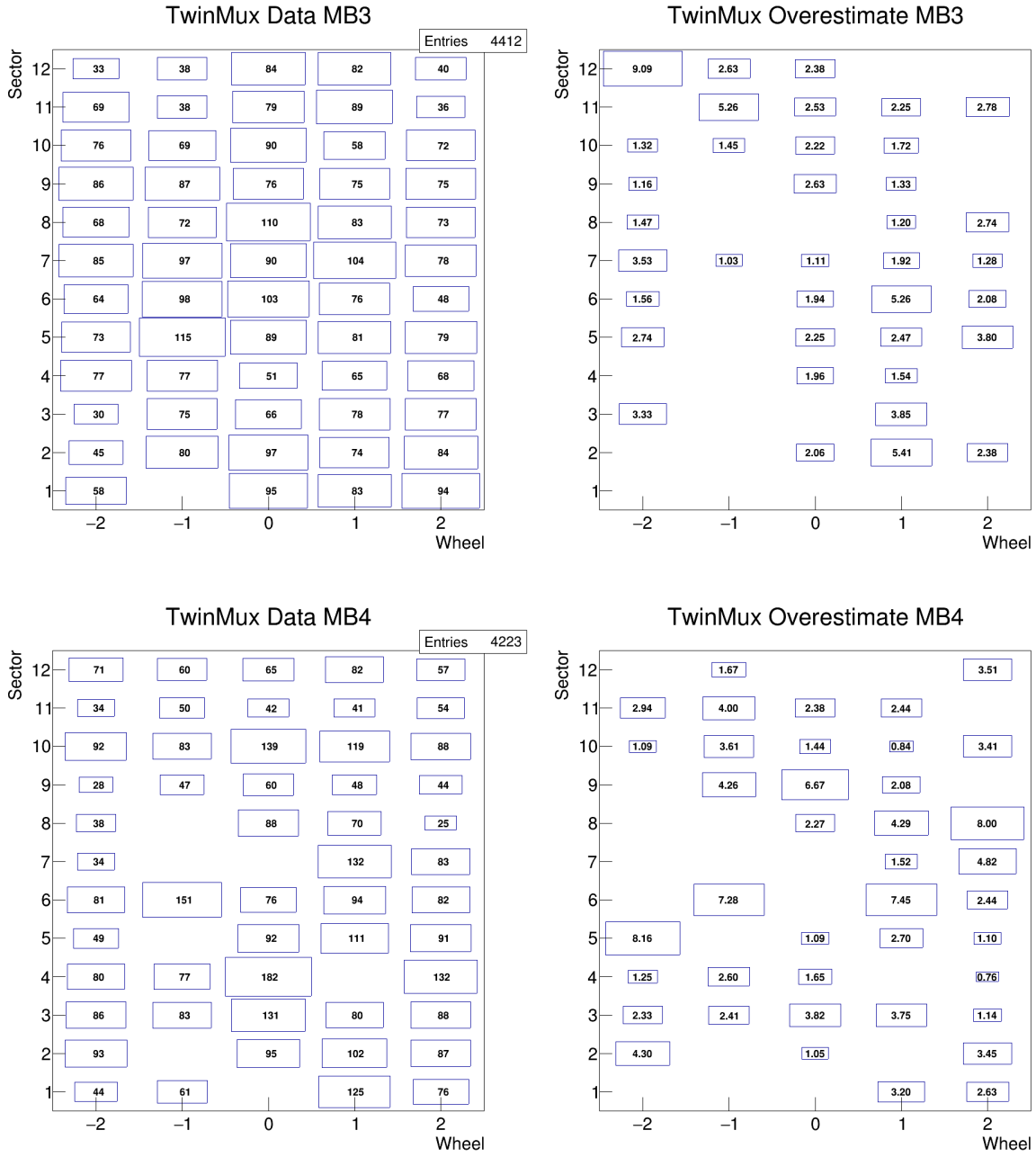

Figure 3.9: Distribution of DT+RPC primitives built by the TwinMux in MB3 (top) and MB4 (bottom) according to their wheel and sector. On the left side there are is the occupancy of the total TwinMux output associated with a single DT input. On the right hand side the percentage of primitives in each wheel and sector where the emulator does not reproduce the hardware behaviour is shown.

3.5.2 BX-ID Comparison in DT+RPC Primitives

As done before, we can now move our attention to the BX identification carried out combining information from both systems. To do that we focus only on the primitives built by the TwinMux hardware and emulator and in the same chamber, in this way

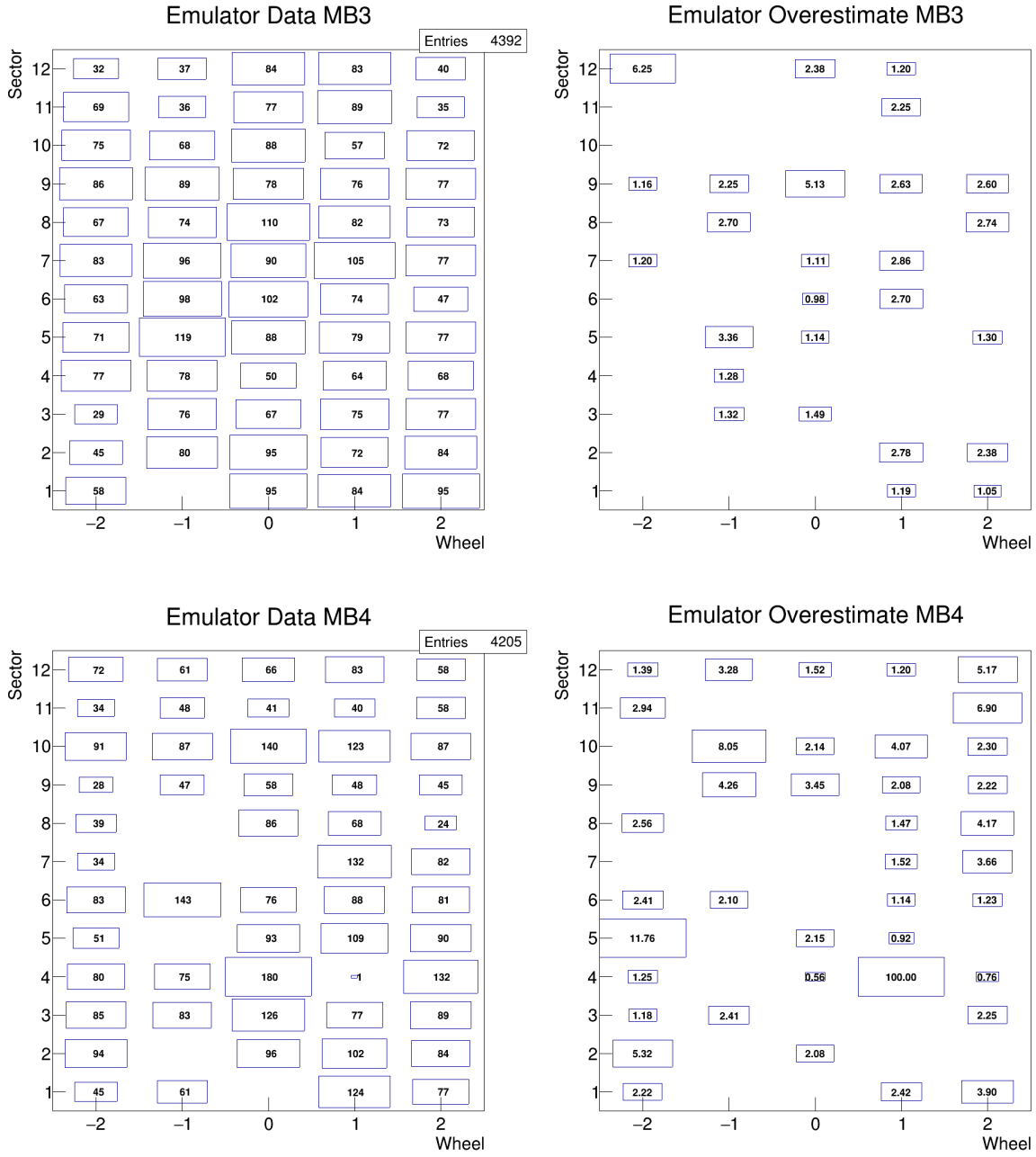

Figure 3.10: Distribution of RPC+DT primitives built by the emulator in MB3 (top) and MB3 (bottom) according to their wheel and sector. On the left side there are is the occupancy of the total emulator output associated with a single DT input. On the right hand side the percentage of primitives in each wheel and sector where the emulator does not reproduce the hardware behaviour are shown.

we can evaluate the fraction of cases where, in a primitive by primitive comparison, disagreements arise. The result of such study is reported in Fig. 3.11, where the emulator's BX identification is compared one to one of the TwinMux and the emulator. From the plot one sees that diagonal comprises the 99.963% of all primitives, leaving only the 0.037% with a different BX between data and emulation. This fraction of events is re-

markably small, showing that the BX correction is performed consistently by hardware and emulator for the selected cases.

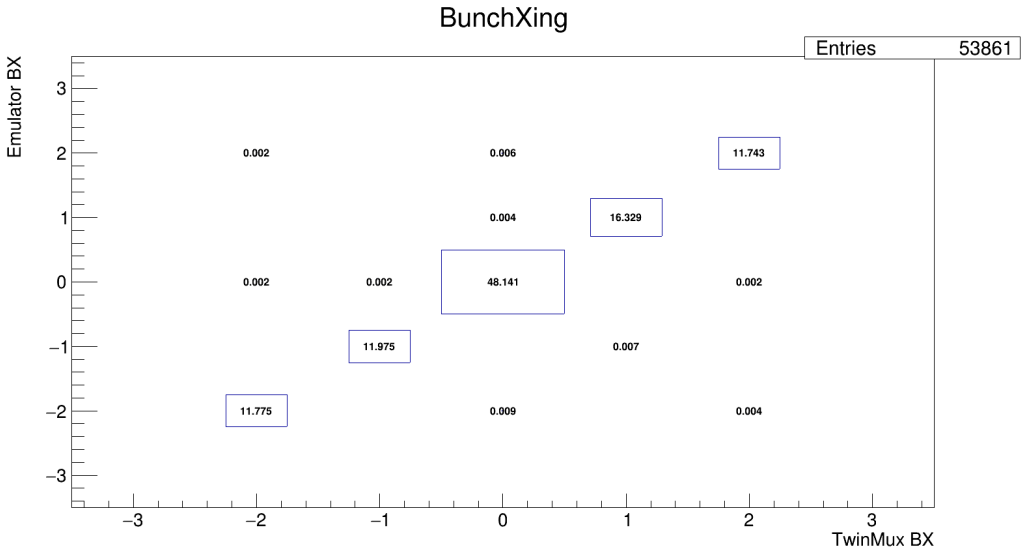

Figure 3.11: One to one comparison of Bunch-Crossing identification between TwinMux and Emulator for DT+RPC primitives contained in both outputs. The fraction of primitives with a different BX-ID in data and emulator output is under 0.1%.

Conclusions

The TwinMux is a system of 60 boards that, since 2016, is part of the Level-1 Muon Trigger of the CMS detector at the LHC. The main task of the TwinMux algorithm is to merge the information coming from two muon detectors, Drift Tubes and Resistive Plate Chambers, in order to provide track segments, also called trigger primitives, to the trigger tracking system of the CMS muon barrel.

In this work we analyze the behaviour of the software emulation of the TwinMux algorithm. A sample of proton-proton collision data enriched in muons, collected by CMS in September 2018, was used to produce emulated TwinMux output and store it together with real TwinMux data and reconstructed objects. A direct data to emulator comparison was carried out, to understand the level of agreement between the hardware and software implementations of the algorithms. Furthermore, the most important figures in terms of physics performance, such as the bunch crossing identification and spatial resolutions, were analyzed and compared.

We developed two selections of trigger primitive objects, aimed at studying the main products of the TwinMux algorithm that enhance the trigger performance: RPC-only primitives, generated when no DT information is available, and DT+RPC primitives, in which the RPC bunch crossing identification complements the DT spatial measurement. In both cases we found the data-emulator agreement to sit around 99%, in line with the expectations considering that the present TwinMux algorithm simulation is not a bit-wise copy of the hardware version. Nevertheless, a geographical analysis pointed to a non completely uniform distribution of the mismatches, that will require further investigation. The bunch crossing assignment in data and emulator was compared and a level of disagreement less than one per mille in both categories was observed.

The spatial resolution of RPC-only primitives was estimated by comparing the track position and direction computed by the TwinMux (hardware and emulator) with the corresponding quantities obtained from track segments reconstructed offline, from full precision Drift Tubes hits. Figures approximately in line with expectations were observed, even if the direction resolution achieved by the emulator is slightly but significantly better than the one found in hardware data. Also this aspect will probably require a follow up study.

In summary, we observed that even if the emulator response does not show a 100% agreement with the hardware, it can be considered accurate, from a statistical perspective, in terms of the physics performance of the trigger system. We conclude that its usage in Montecarlo simulations is appropriate, while it cannot be fully trusted for the monitoring and qualification of the hardware. Further investigation of the main differences we have found could provide the insight needed to improve the emulator implementation and reach an agreement with data very close to 100%.

Bibliography

[1] L. Guiducci, *Design and Test of the Off-Detector Electronics for the CMS Barrel Muon Trigger*, PhD Thesis, March 2006

[2] CMS Collaboration, *Performance of the CMS TwinMux Algorithm in late 2016 pp collision runs*, CERN-CMS-DP-2016-074, 16 December 2016

[3] CMS Collaboration, *The inclusion of RPC only segments in the Barrel Muon Track Finder*, CERN-CMS-DP-2018/007, 02 February 2018

[4] CMS Collaboration, *Performance of the CMS muon detector and muon reconstruction with proton-proton collisions at* $\sqrt{s}$ *= 13 TeV*, arXiv:1804.04528v2 [physics.ins-det], 20 June 2018

[5] CMS Collaboration, *The CMS Barrel Muon trigger upgrade*, 2017 JINST 12 C01095

[6] `https://github.com/cms-sw/cmssw/tree/master/L1Trigger/L1TTwinMux`

[7] `https://github.com/cms-sw/cmssw/blob/master/DQM/DTMonitorModule/src/DTTrigGeomUtils.cc`

[8] `https://github.com/cms-sw/cmssw/blob/CMSSW_10_2_X/DPGAnalysis/Skims/python/ZMuSkim_cff.py`

[9] `https://root.cern.ch/`